JOURNAL OF MATERIALS SCIENCE 30 (1995) 5901–5909

Comparison of the effectiveness of rare-earth sintering additives on the high-temperature stability of α-sialon ceramics

H. MANDAL, N. CAMUŞCU, D.P. THOMPSON
Materials Division, Department of Mechanical, Materials and Manufacturing Engineering, University of Newcastle upon Tyne, Newcastle upon Tyne, NE1 7RU, UK

α-sialon starting compositions with $m = 1$ and $n = 1.7$ have been densified by either hot-pressing or pressureless sintering using Y_2O_3 and Ln_2O_3 additions where Ln is neodymium, samarium, dysprosium or ytterbium. The resulting materials have been heat treated at 1450 °C to crystallize the grain-boundary liquid into crystalline oxynitride phases. The effect of sintering additive on the design of final properties has been studied and Dy_2O_3 was found to be the best sintering additive to obtain desirable properties for α-sialon and also α–β sialon materials.

1. Introduction

Sialon ceramics offer advantages of easier fabrication compared with Si_3N_4 ceramics because of the lower viscosity of the M–Si–Al–O–N liquid phase which facilitates easier densification at sintering temperatures. Another advantage is that the amount of intergranular phase can be reduced if the transient liquid phase is absorbed into the matrix forming α-sialon phase in the final product [1, 2].

Pressureless sintered β-sialons were the first nitrogen ceramics to achieve large-scale commercial viability. This was because the presence of alumina in the starting mix lowers the eutectic temperature of the densifying liquid phase by some 200–300 °C, making it possible to achieve full density by pressureless sintering and allowing complex-shaped components to be prepared easily in large numbers and at lower cost. The resulting β-sialon materials have a Young's modulus of ≈300 GPa, strengths of up to 1000 MPa and K_{IC} values up to 8 MPa $m^{1/2}$ [3].

α-sialon, unlike β-sialon, can accommodate additional cations into its structure because the unit cell contains two large interstices and the general formula for α-sialons is $M_xSi_{12-(m+n)}Al_{m+n}O_nN_{16-n}$ where $x < 2$ and M is lithium, calcium, yttrium, and lanthanides with $z > 60$ [4]. These materials offer at least two useful advantages over β-sialons:

1. they provide the possibility of producing single-phase sialon ceramics with a minimum of grain-boundary phase, because the metal oxide present in the starting mix promotes the formation of a liquid phase which densifies the material and at firing temperatures can be incorporated into the α-sialon structure;
2. the product shows increased hardness.

Mixed two-phase sialon ceramics offer possibilities of tailoring the microstructure, for example, equiaxed α-sialon grains can be matched with elongated β-sialon grains to form a toughened composite, and consequently the properties of the final product can be improved, because they combine the high fracture toughness of β-sialon with the good hardness of an α-sialon. Another advantage of multi-phase sialon compositions is that densification is much easier than for pure α-sialon [5].

Although it is desirable to incorporate all the lanthanum atoms in the starting mix in the final α-sialon structure, this is very difficult and a certain fraction remain as a residual Ln–Si–Al–O–N intergranular glassy phase which degrades the mechanical and chemical properties of the material above the glass softening temperature (900–1100 °C).

Heat treatment is one of the accepted methods for eliminating (or minimizing) the grain-boundary glass in nitrogen ceramics by converting it into refractory crystalline phase(s) thus improving the high-temperature properties [6, 7]. Recent studies have found that heat treatment above the eutectic temperature of sialon materials (e.g. $T > 1400$ °C) promotes melting of grain-boundary glass and facilitates a reaction between the grain-boundary liquid and sialon grains, resulting in the formation of a more refractory, aluminium-containing nitrogen-melilite solid solution (M'_{ss}) phase at grain boundaries [8, 9].

To optimize the final properties of the material, design of the starting compositions is very important to achieve final desired properties. However, there are several factors which must be optimized, two of which are of primary importance.

1. Chemical stability of the α-sialon phase with respect to the sintering additive used; the chosen sintering additive for producing α-sialon or α–β sialon should satisfy the following criteria [10] :

0022–2461

(a) the lanthanide cation must be able to stabilize the α-sialon structure;

(b) the eutectic temperature of the oxide-containing liquid should be lower than the formation temperature of the α-sialon phase but high enough to give good creep behaviour;

(c) no intermediate phase produced by the oxide during sintering should remain in the final product and hinder densification;

(d) it is desirable but not essential to have a high solubility of nitrogen in the liquid-phase region in the Ln–Si–Al–O–N system in equilibrium with the α-sialon phase;

(e) the crystalline phases devitrified from the lanthanum-containing grain-boundary glass should be oxidation and high-temperature resistant.

2. Thermal stability of α-sialon with respect to the heat-treatment temperature [11]; recent work at Newcastle has shown that in some sialon compositions densified with rare-earth oxides, the α-sialon phase formed at normal sintering temperatures (1750–1800 °C) is unstable at lower (< 1550 °C) temperatures and transforms to a mixture of β-sialon plus either a crystalline or glassy grain-boundary phase. The kinetics of the transformation are so slow below 1200 °C that optimized materials can be used up to this temperature, but at higher temperatures, especially above the eutectic temperature, some change in mechanical properties will start to occur because of $\alpha \rightarrow \beta$ sialon transformation.

In the present work, α-sialon starting compositions have been densified by either hot pressing or pressureless sintering using Ln_2O_3, where Ln is neodymium, samarium, dyprosium, ytterbium and also Y_2O_3. The resulting materials have been heat treated at 1450 °C to crystallize the grain-boundary phase. The effect of different rare-earth oxide additives on densification, $\alpha \rightleftharpoons \beta$ sialon transformation, mechanical properties and especially the ability to achieve designed properties, has been investigated.

2. Experimental procedure

Four rare-earth elements, neodymium, samarium, dysprosium, ytterbium, and yttrium, were selected for preparation of α-sialon ceramics. The starting compositions in different systems are very similar (Table 1) and resemble compositions in the α-sialon phase region with the overall composition $(Y, Ln)_{0.333}Si_{9.3}Al_{2.7}O_{1.7}N_{14.3}$ where $m = 1$ and $n = 1.7$. The reason for this specific composition is to give enhanced α-sialons sinterability by pressureless sintering. Graphical representations of the starting composition are shown in Fig. 1. Although the weight percentage of rare-earth oxides increases a little as the atomic number of the lanthanide elements increases, in mole ratio, the amount of Ln_2O_3 in different samples is exactly the same.

Sialon compositions were prepared using powder mixtures of Si_3N_4 (HC Stark-Berlin, Grade LC10), AlN (HC Starck-Berlin, Grade A), Al_2O_3 (Alcoa, Grade A16SG), Ln_2O_3 (99.9%, Sigma Chemical Company Ltd) and Y_2O_3 (99.9%, HC Starck-Berlin). The rare-earth oxides were calcined at 1000 °C for 4 h before use, to remove any absorbed water. When calculating the compositions, 3.5% SiO_2 and 3.5% Al_2O_3 on the surfaces of Si_3N_4 and AlN, respectively, were taken into account.

The starting materials were mixed in water-free isopropanol and milled in an agate mortar for 45 min. The reason for using this method was to avoid segregation of rare-earth oxides during drying. The size of each batch used was 15 g. After drying and sieving, powders were compacted into pellets (about 3 g) by pressing uniaxially and then isostatically under 200 MPa. Before firing, the specimens were embedded in micrometre-sized boron nitride powder in graphite crucibles and sintered in a carbon resistance furnace at 1800 °C for 2 h under a protective nitrogen atmosphere, and then the furnace was cooled at a rate of 50 °C min^{-1} from 1800 °C to 1200 °C. The green pellets were also hot pressed in BN-coated graphite dies at 1800 °C for 1 h. All sintered materials were placed in a carbon crucible and re-heated up to 1800 °C in a smaller size pressureless sintering furnace for 20 min and quenched (400 °C min^{-1}) to room temperature. Heat treatment was carried out for all samples in an alumina tube furnace at 1450 °C for up to 168 h (1 week) under a nitrogen gas atmosphere.

Product phases were characterized by X-ray diffraction (XRD) using a Hägg–Guinier camera and CuK_{α_1}

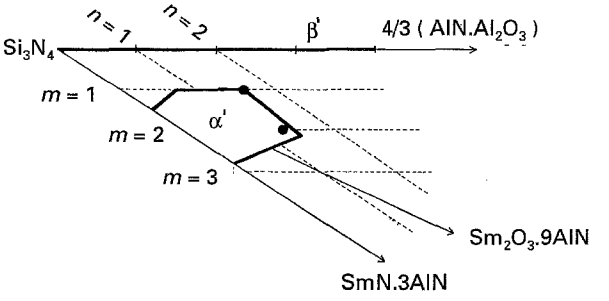

Figure 1 α-sialon plane, showing the starting compositions used in this study.

TABLE I Starting compositions of different Ln (Y)–α-sialon ceramics

Sample	Si_3N_4	Al_2O_3	AlN	Nd_2O_3	Sm_2O_3	Dy_2O_3	Yb_2O_3	Y_2O_3
Nd2	71.82	3.40	15.55	9.23	–	–	–	–
Sm2	71.58	3.39	15.50	–	9.53	–	–	–
Dy2	71.10	3.37	15.40	–	–	10.13	–	–
Yb2	70.70	3.35	15.31	–	–	–	10.64	–
Y2	74.06	3.51	16.04	–	–	–	–	6.39

radiation. The computer-linked line scanner (SCANPI LS-20) system, developed by Werner (Arrhenius Laboratory, University of Stockholm, Sweden) was used for direct measurements of X-ray films and refinement of lattice parameters. The amounts of α- and β-sialon phases were found by quantitative estimation from the XRD pattern using the integrated intensities of the (1 0 2) and (2 1 0) reflections of α-sialon and the (1 0 1) and (2 1 0) reflections of β-sialon in the following equation

$$\frac{I_\beta}{I_\alpha + I_\beta} = \frac{1}{1 + K[1/W_\beta) - 1]} \quad (1)$$

where I_α and I_β are observed intensities of α- and β-sialon lines, respectively. W_β is the relative weight fraction of β-sialon. K is the combined proportionality constant resulting from the constants in the two equations, namely

$$I_\beta = K_\beta W_\beta \quad (2)$$

$$I_\alpha = K_\alpha W_\alpha \quad (3)$$

which is 0.518 for β(1 0 1) – α(1 0 2) reflections and 0.544 for β(2 1 0) – α(2 1 0) reflections [12].

After application of a gold coating, polished surfaces of as-sintered and heat-treated samples were examined using a Camscan S4-80 DV scanning electron microscope (SEM) equipped with EDX facilities and a windowless detector suitable for light element analysis.

Hardness (HV10) and indentation fracture toughness, K_{IC}, measurements were made at room temperature using a Vickers diamond indentor with a 98 N (10 kg) load, and fracture toughness was evaluated according to the method of Evans and Charles [13].

Oxidation resistance tests were performed in a Carbolite muffle furnace in air using 24 h at 1450 °C. The results were examined visually and by measuring the weight change of samples.

3. Results

3.1. Densification

Table II gives densities of different samples after sintering under different conditions. Examination of polished cross-sections of the hot-pressed sialon ceramics by SEM showed only very few micro-pores to be present, indicating that the samples had reached virtually theoretical density after hot-pressing. Therefore the measured densities of the hot-pressed samples were used as a reference for determining the extent of densification of pressureless sintered materials of the same overall composition.

The major concern in densification of α-sialon materials by pressureless sintering is to find a sintering additive which can stabilize the α-sialon structure and at the same time promote a fluid transient liquid which can densify the material.

It can be seen from the table that for pressureless sintered samples, the highest densities of 96.4% of theoretical were obtained using Dy_2O_3 and Sm_2O_3 as sintering additives. The poor sinterability of Yb_2O_3 and Y_2O_3 is believed to be due to the higher eutectic temperature in these systems. Although compositions in the samarium–sialon system gave the highest densities, even better results could have been obtained in this system because of the reasons explained below (Table III). In the case of compositions in the neodymium and samarium systems, the considerably lower densities than expected, were attributed to the high melting temperature of the neodymium- samarium-M' phase formed during sintering (see Table III). M' is always an intermediate product in the samarium and neodymium α-sialon systems during sintering and incorporates large amounts of sintering additive (neodymium or samarium) into its structure; as a result, the densification of α-sialon materials is significantly retarded until the M' phase melts and provides more liquid phase for sintering [8]. Because M' does not occur in the dysprosium system for this specific composition, and the eutectic in the Dy_2O_3 system is lower than in the Yb_2O_3 and Y_2O_3 systems, compositions in the dysprosium-sialon system give better final densities.

Typical back-scattered SEM images of compositions densified with Dy_2O_3 and Yb_2O_3 by pressureless sintering at 1800 °C are given in Fig. 2 to illustrate the porosity in pressureless sintered samples and also the difference between the two sintering additives.

3.2. Phase analysis and microstructural studies of sintered materials

In all samples, α-sialon is the predominant phase and no other crystalline phase(s) appeared in the grain boundaries on cooling except in pressureless sintered neodymium and samarium compositions. The relative amounts of α and β-sialon phases after sintering were established by XRD and the results are presented in Table III. Although all starting compositions aimed to produce 100% α-sialon, only Dy_2O_3, Yb_2O_3 and Y_2O_3 additions gave results close to the designed composition, while Nd_2O_3 and Sm_2O_3 additions gave only ≈50% and ≈75%, respectively.

TABLE II Densities of Ln(Y)-containing samples sintered at 1800 °C either by hot pressing or pressureless sintering

Sintering conditions	Sintering Additives									
	Nd_2O_3		Sm_2O_3		Dy_2O_3		Y_2O_3		Yb_2O_3	
	ρ ($g\,cm^{-3}$)	%TD	ρ ($g\,cm^{-3}$)	%TD	ρ ($g\,cm^{-3}$)	%TD	ρ ($g\,cm^{-3}$)	%TD	ρ ($g\,cm^{-3}$)	%TD
Hot pressed	3.354	100	3.367	100	3.378	100	3.280	100	3.398	100
Pressureless	3.196	95.3	3.246	96.4	3.256	96.4	3.120	95.1	3.220	94.8

TABLE III X-ray results of samples sintered at 1800 °C either by hot pressing or pressureless sintering

Sample	α′ (%)	β′ (%)	Other
Nd2 (HP)	m(58)	m(42)	21R(w)
Nd2 (PS)	m(50)	m(50)	M′(w), 21R(w)
Sm2 (HP)	s(70)	mw(30)	21R(w)
Sm2 (PS)	s(77)	mw(23)	M′(vw), 21R(w)
Dy2 (HP)	vs(100)	(0)	21R(vw)
Dy2 (PS)	vs(97)	vvw(3)	21R(vw)
Yb2 (HP)	vs(91)	vw(9)	21R(vw)
Yb2 (PS)	vs(100)	(0)	21R(vw)
Y (HP)	s(90)	w(10)	21R(w)
Y (PS)	vs(95)	vw(5)	21R(w)

Note: for X-ray peak intensities, s = strong, m = medium, w = weak, v = very, numbers in brackets are relative percentages of α- and β-sialon phases.

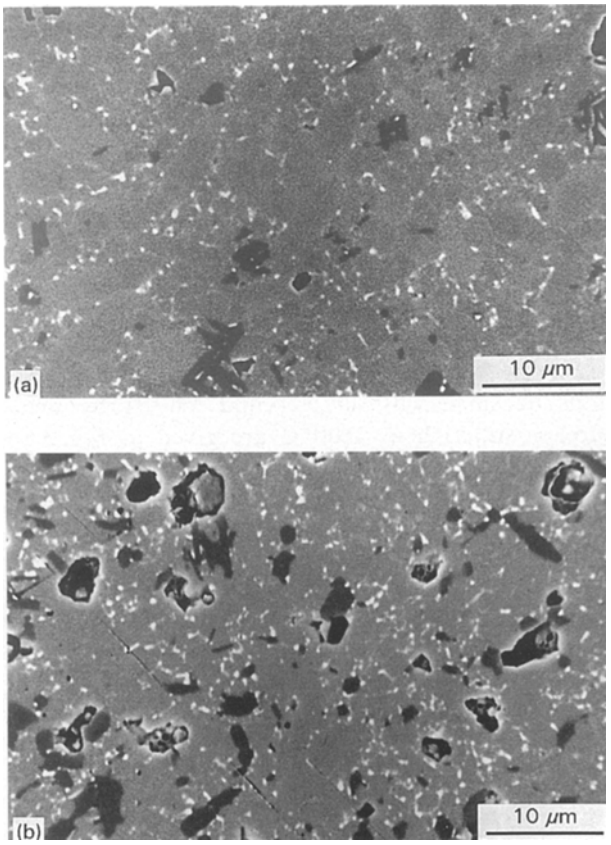

Figure 2 Microstructures of (a) Dy_2O_3 and (b) Yb_2O_3 samples densified at 1800 °C by pressureless sintering.

A number of back-scattered scanning electron micrographs were examined using polished cross-sections of sintered specimens (see Fig. 3). Because the contrast on back-scattered electron micrographs depends mainly on the mean atomic number, micrographs very clearly distinguish between various phases; the β-sialon and 21R grains (which contain no rare-earth element) are black and more needle-like, whereas the α-sialon grains (which contain a small amount of rare-earth element) are grey and more equiaxed whilst lanthanum-rich crystalline or glassy phases appear fine grained and white, because of the

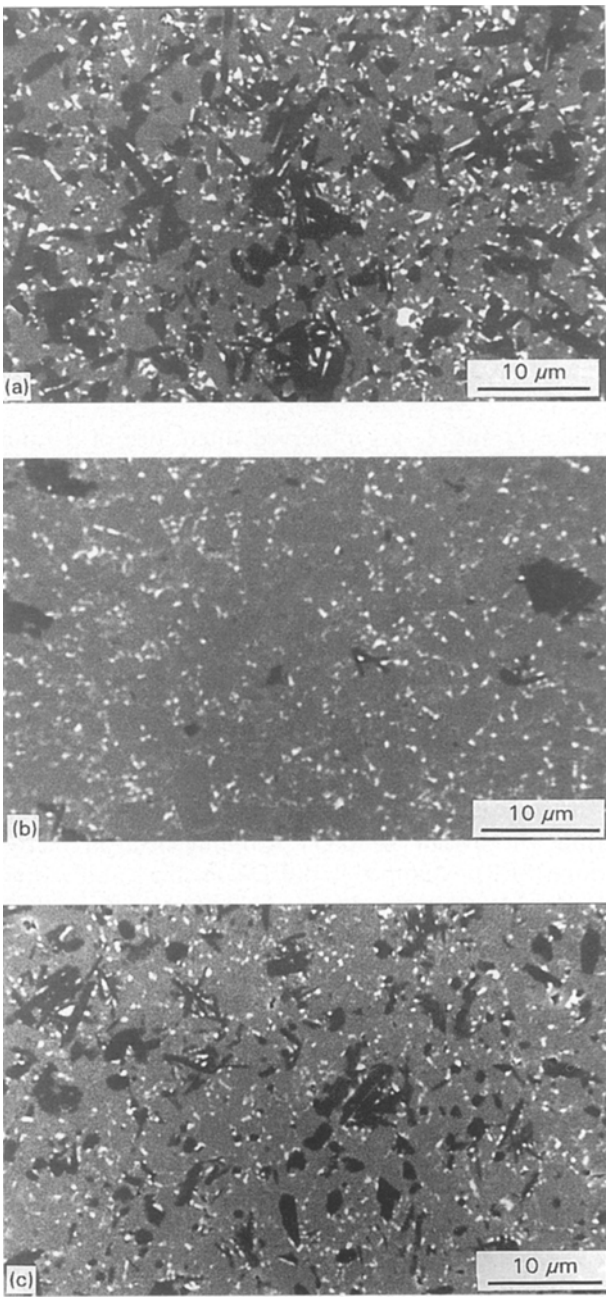

Figure 3 Back-scattered scanning electron micrographs of hot-pressed α-sialon samples densified by (a) Nd_2O_3, (b) Dy_2O_3 and (c) Yb_2O_3.

high lanthanum content. Two points can be clearly distinguished on moving to lower Z rare-earth additives, namely, that the α-sialon content decreases, and the amount of intergranular phases increases.

The explanation for the decrease in α-sialon content correlates with the relative sizes of the rare-earth metal dopants (not yttrium) of the sintering additives, so that ytterbium and dysprosium form more α-sialon whereas neodymium and samarium form less. Because the solubility of nitrogen in Y–Si–Al–O–N liquids (≈16 at%) is lower than in rare-earth systems (≈20 at%) [14], the amount of α-sialon precipitated in yttrium-containing compositions is less than in the ytterbium and dysprosium systems. Clearly, the explanation for the increase in the amount of intergranular phase for low atomic number rare-earth additives is related to the low α-sialon content, because

α-sialons incorporate some of the densification additives(s) into the crystal structure as a result of which, the quantity of residual glass in the grain boundaries decreases with increasing α-sialon content. Therefore the amount of residual glass in samples densified with Dy_2O_3, Yb_2O_3 and Y_2O_3 additives are considerably less than in Sm_2O_3 and especially Nd_2O_3 densified compositions.

3.3. Phase analysis and microstructure of heat-treated samples

Glasses form metastably during fast cooling of viscous liquids from the liquid state. The phase transformation from an amorphous to a crystalline state reduces the free energy of the system and therefore takes place spontaneously at temperatures when the energy barrier for atomic diffusion can be overcome.

For the materials studied in this work, devitrification of the grain-boundary glass occurred readily at 1000 °C. However, the stability of the devitrified phases varies in different systems and a full discussion has been given previously [15]. In the present paper, crystallization of grain-boundary sialon liquids at temperatures above the eutectic is discussed. This is always accompanied by α⇌β transformation.

All samples were heat treated at 1450 °C in nitrogen for up to 168 h (1 week) in order to study effects of prolonged heat treatments on the phase content of the samples and especially α⇌β transformation. The X-ray results in Table IV and Fig. 4 show that α-sialon, β-sialon and 21R are the predominant phases after heat treatment. In addition, *M'*-phases in the neodymium and samarium systems and a garnet phase in the yttrium system, were observed with an increasing amount of α → β sialon transformation occurring according to the following reaction

$$\alpha\text{-sialon} + \text{liquid}(L_1) \rightarrow \beta\text{-sialon} + \text{grain-boundary phase (M' or garnet)} + \text{liquid}\ (L_2) \quad (4)$$

where compositions of L_1 and L_2 are different. The mechanism of this transformation is discussed in detail elsewhere [16].

It is very clear from the results that neodymium and samarium α-sialons readily undergo this reaction. Although the neodymium and samarium systems produce *M'*-phase, which is an excellent grain-boundary phase for α- and α–β sialon ceramics [9], *M'* formation is unfortunately accompanied by α → β sialon transformation which increases the amount of liquid phase content in the sialon material. Therefore, in neodymium and samarium compositions the α-sialon content gradually decreases as the heat-treatment time increases and α-sialon completely disappears in both systems after 168 h (1 week) at 1450 °C. At the same time, the amount of *M'*-phase also increases. However, the degree of increase in *M'* content is much less than that of β-sialon, and this suggests that not all the metal cations that have been released from the α-sialon structure during α → β sialon transformation have been used in *M'* formation. A fraction of these metal cations have remained in the glass.

In the case of Dy_2O_3 and Yb_2O_3 additions, α-sialon is more stable than in the neodymium and samarium systems and after 168 h heat treatment at the same temperature, very little transformation was observed.

The changes in microstructure were investigated by examining back-scattered scanning electron micrographs of neodymium, dysprosium and ytterbium samples after 24 and 168 h heat treatment at 1450 °C, and the results are illustrated in Fig. 5. Systematic

TABLE IV X-ray results of samples after heat treatment at 1450 °C for different times $m = 1$ $n = 1.7$ 100% α-sialon composition

Sample	HT time (h)	α' (%)	β' (%)	Other
Nd2 (PS)	24	mw (24)	s (76)	21R(w), M'(m)
	72	vw (5)	vs (95)	21R(w), M'(m)
	168	0	vs (100)	21R(w), M'(m)
Nd2 (HP)	24	m (34)	s (66)	21R(mw), M'(m)
	168	0	vs (100)	21R(w), M'(m)
Sm2 (PS)	24	s (63)	mw (27)	21R(w), M'(w)
	72	m (40)	ms (60)	21R(w), M'(mw)
	168	0	vs (100)	21R(w), M'(mw)
Sm2 (HP)	24	ms (45)	ms (55)	21R(w), M'(mw)
	168	0	vs (100)	21R(w), M'(mw)
Dy2 (PS)	24	vs (96)	vw (4)	21R(vw)
	72	vs (91)	vw (9)	21R (vw)
	168	vs (90)	w (10)	21R(vw)
Dy2 (HP)	24	vs (97)	vw (3)	21R (vw)
	168	vs (86)	w (14)	21R (vw)
Yb2 (PS)	24	vs (100)	0	21R (vw)
	72	vs (96)	vw (4)	21R(vw)
	168	vs (96)	vw (4)	21R (vw)
Yb2 (HP)	24	vs (86)	w (14)	21R(vw)
	168	s (78)	mw (22)	21R(vw)
Y2 (PS)	24	vs (93)	vw (7)	21R(w), G(vw)
	72	vs (90)	w (10)	21R(w), G(w)
	168	vs (86)	w (14)	21R(w), G(w)
Y2 (HP)	24	s (82)	mw (18)	21R(w), G(vw)
	168	s (70)	m (30)	21R (w), G(w)

Note: for X-ray peak intensities, s = strong, m = medium, w = weak, v = very; numbers in brackets are relative percentages of α- and β-sialon phases. G = garnet ($Y_3Al_5O_{12}$).

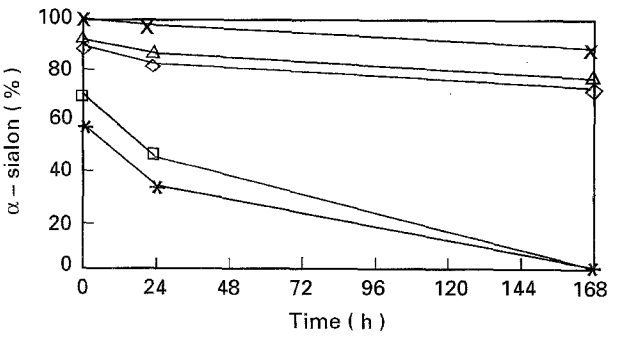

Figure 4 The α-sialon: (α + β-sialon) ratio in samples heat treated at 1450 °C as a function of heat-treatment time. (*) Nd, (□) Sm, (×) Dy, (◇) Y, (Δ) Yb.

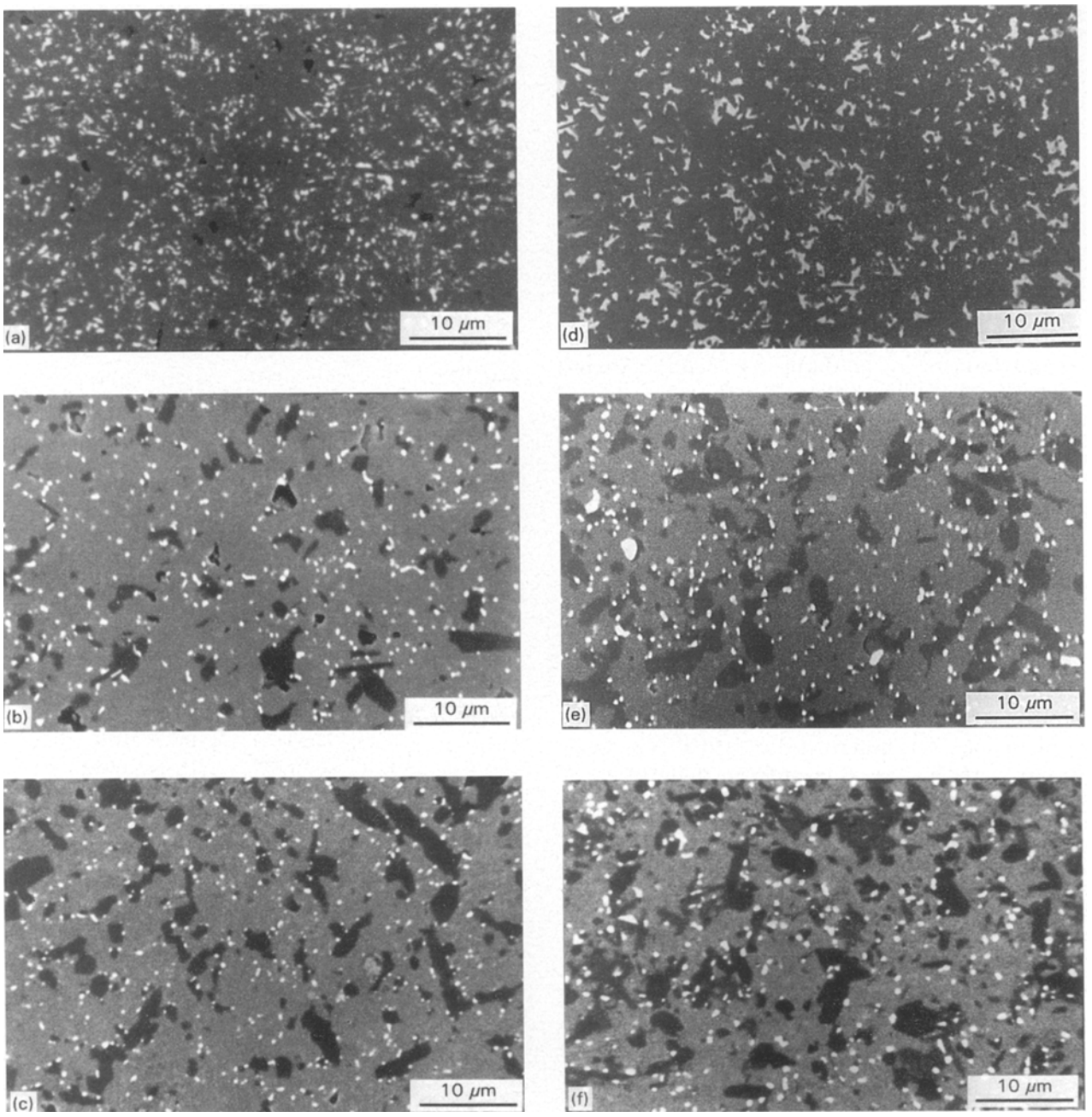

Figure 5 SEM back-scattered images of (a) Nd, (b) Dy, (c) Yb samples heat-treated at 1450 °C for 24 h and (d) Nd, (e) Dy, (f) Yb samples heat treated at 1450 °C for 168 h.

differences were observed for neodymium samples with increasing time and also compared with the microstructure after sintering. Sintered samples contained mainly α-sialon grains surrounded by grain-boundary glass and elongated β-sialon grains. However, heat-treated samples showed enlarged β-sialon grains and more crystallization of *M'*-phase as the heat-treatment time increased. No significant change was observed in the microstructure of samples densified with Dy_2O_3 or Yb_2O_3.

3.4. Mechanical properties

Because the densification of pressureless sintered samples was incomplete, only hot-pressed samples were tested for hardness and toughness and the results are summarized in Figs 6 and 7 in terms of heat-treatment time. It can be seen very clearly from the hardness graph that hardness decreases with increasing time because this is related to the amount of α-sialon and, as explained in previous sections, the $\alpha \rightarrow \beta$ sialon transformation increases with increasing time. Therefore, the hardness of neodymium and samarium samples reduced significantly with time, while other systems (especially Dy_2O_3) showed very little change.

The fracture toughness of sialon ceramics can be correlated with grain shape, and high aspect ratio β-sialon microstructures show the best toughness. Crack deflection is therefore the most predominant mechanism for toughening. Because the current microstructural observations in Section 3.3 showed, especially for neodymium and samarium compositions, α-sialon grains initially splitting into smaller, more elongated grains of β-sialon, toughness improves

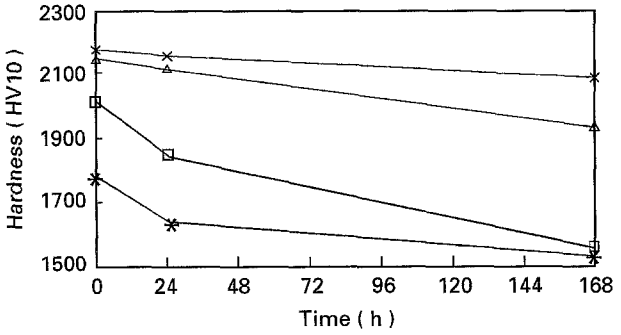

Figure 6 Vickers hardness (HV10) of samples as a function of heat-treatment time. (*) Nd, (□) Sm, (×) Dy, (Δ) Yb.

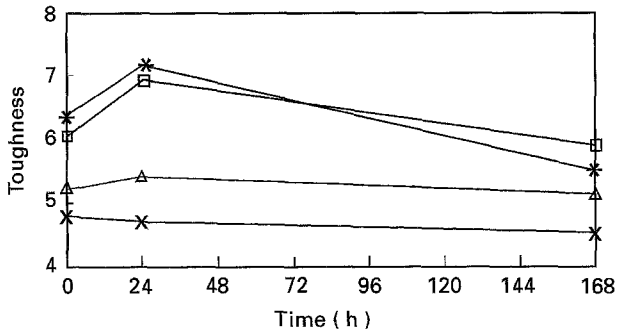

Figure 7 Fracture toughness of samples as a function of heat-treatment time. (*) Nd, (□) Sm, (×) Dy, (Δ) Yb.

slightly but then drops, as the size of β-sialon and M'-grains increases with increasing heat-treatment time, and therefore the toughness decreases. Because no significant change in the microstructures of samples densified with dysprosium, yttrium and ytterbium additions occurs, no significant change in toughness in dysprosium, yttrium and ytterbium compositions is observed.

3.5. Oxidation resistance

Oxidation tests were performed at 1450 °C for 24 h in air for both sintered and heat-treated neodymium, samarium and dysprosium samples. No significant difference in oxidation resistance of sintered and heat-treated samples was observed. Both neodymium and samarium samples oxidized significantly and the neodymium sample was almost totally destroyed. Although the crystalline phase in both systems after heat treatment was the M'-phase, a certain amount of undevitrified glassy phase also remained due to $\alpha \rightarrow \beta$ sialon transformation. This is not surprising because the starting composition corresponded to a pure α-sialon, and as only a certain amount was produced, the remaining oxides and nitrides remaining in the liquid phase were of composition not equivalent to M'-phase. Also the test temperature, 1450 °C, resulted in more transformation. However, the situation is different in the case of dysprosium samples. Both sintered and heat-treated samples showed a negligible weight increase with the formation of a thin layer of cristobalite on the surface of the samples.

These observations clearly show how the properties of these materials are significantly affected if the designed composition cannot be achieved.

4. Discussion

Similar starting compositions designed to produce single-phase α-sialon materials using five different rare-earth oxides have been explored. However, it can be clearly seen from the results presented here that it was very difficult to obtain the desired composition, more so with certain rare-earths than with others. This can be explained in terms of the ionic radius of the rare-earth cations [17] and the increased tendency for α-sialon formation as the ionic radius of the rare-earth cation decreases. Therefore, for Dy_2O_3 additions, nearly all the dysprosium atoms go into the α-sialon structure while for Nd_2O_3 additions, very few neodymium atoms go into the α-sialon structure. This implies that especially in the Nd_2O_3 and Sm_2O_3 systems, neodymium and samarium cations go into the liquid and remain as a glassy or crystalline phase after cooling and this glass will soften above the glass transition temperature and severely degrade the high-temperature properties of these materials. Above the eutectic temperature, the glass will melt to produce a liquid again, which will facilitate the $\alpha \rightleftharpoons \beta$ sialon transformation. Therefore, Nd_2O_3 and Sm_2O_3 are not the best sintering additives for α-sialon and α–β sialon ceramics.

Another α-sialon composition [18] with $m = 2$ and $n = 1.5$ located in the α-sialon region (see Fig. 1) was prepared using Dy_2O_3 and Nd_2O_3 as sintering additives to obtain a better understanding of the effect of sintering additive on the design of properties. Samples were prepared by the same method mentioned in previous sections. X-ray phase analysis of samples after sintering and heat treatment resulted in Dy_2O_3 densified composition giving nearly pure α-sialon and the resulting material showing very little $\alpha \rightarrow \beta$ transformation after heat treatment (see Fig. 8) whereas 83% α-sialon–17% β-sialon was observed for Nd_2O_3 compositions and the resulting materials showed nearly complete transformation to β-sialon after 168 h of heat treatment (see Fig. 9).

In the case of Yb_2O_3 and Y_2O_3-densified materials, the main problem is the difficulty of obtaining densification and also the high cost of Yb_2O_3, which is the most expensive sintering additive in the systems used in this research.

From the above discussion, Dy_2O_3 has notably superior advantages compared to the rest of the additives because:

(a) it gives easier densification;
(b) it gives the desired final products after sintering;
(c) it gives the best microstructure and hence mechanical properties after sintering;
(d) it shows very little $\alpha \rightleftharpoons \beta$ sialon transformation;
(e) it retains the designed composition during heat treatment;
(f) it displays better oxidation resistance even without heat treatment; and
(g) it is cheaper than Sm_2O_3 or Yb_2O_3.

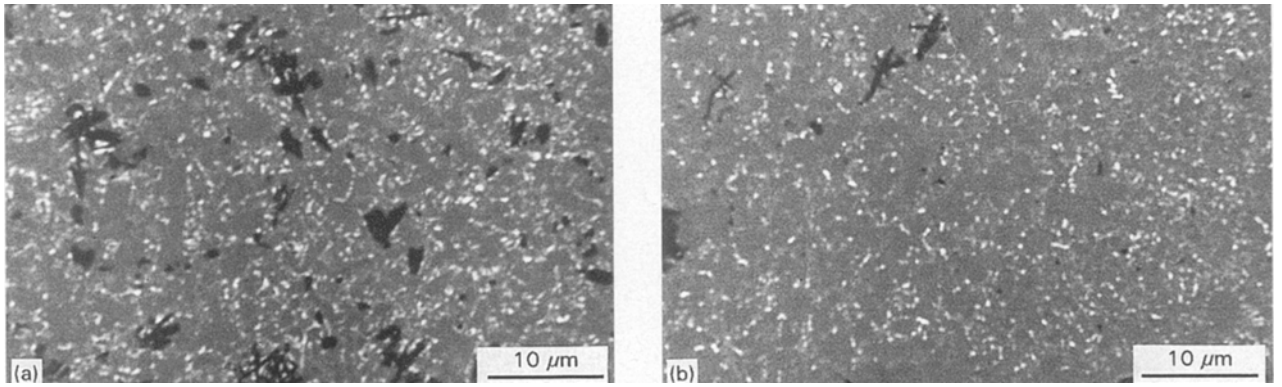

Figure 8 Back scattered scanning electron micrographs of (a) Nd_2O_3 and (b) Dy_2O_3 densified samples.

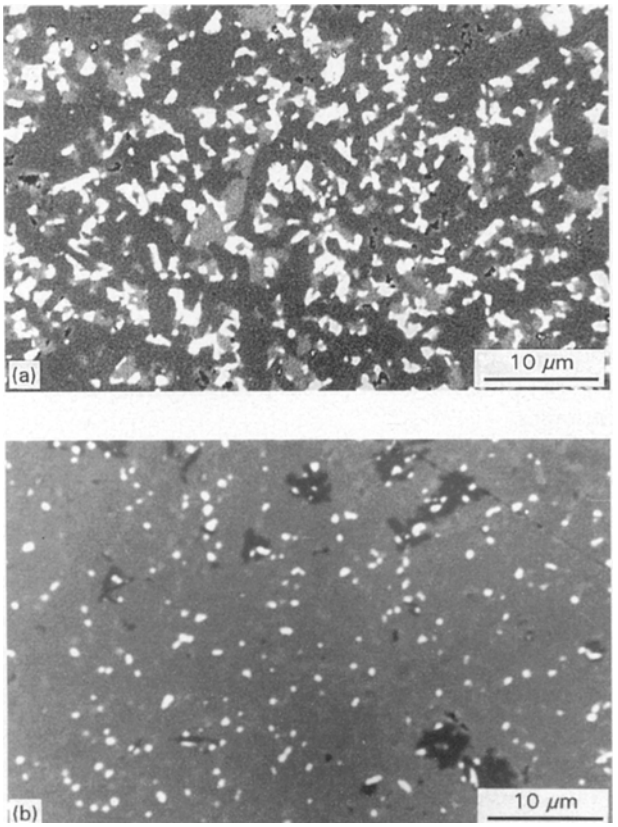

Figure 9 Back scattered scanning electron micrographs of (a) Nd_2O_3 and (b) Dy_2O_3 samples heat treated at 1450 °C for 168 h.

5. Conclusion

Nd_2O_3 and Sm_2O_3 are comparatively large cation-size sintering additives which do not readily form pure α-sialon materials. As a result, there remains an excessive amount of glassy phase in the structure after sintering. It is believed that the residual glass facilitates $\alpha \rightarrow \beta$ sialon transformation at elevated temperatures ($> 1400\,^{\circ}C$). $\alpha \rightarrow \beta$ sialon transformation in turn increases the amount of glass in the material because of the cations released from the α-sialon structure. This procedure then iterates cyclically, i.e. glass results in more $\alpha \rightarrow \beta$ transformation which in turn results in more glass. Ultimately this would result in failure if these materials were used in high-temperature engineering applications, because of oxidation and creep. Although the neodymium and samarium systems produce M'-phase which is an excellent grain-boundary phase for α- and $\alpha + \beta$ sialon ceramics, the inevitable $\alpha \rightarrow \beta$ sialon transformation in these systems decreases their reliability and results in worse high-temperature performance.

Dysprosium and ytterbium (and also yttrium) α-sialon systems are more stable at elevated temperatures because of their small cation size. Although they do not produce M' phase in the specific compositions used here, $\alpha \rightarrow \beta$ sialon transformation does not occur. Densification with these additives is expected to be more difficult when compared with neodymium and samarium systems, but dysprosium gave the highest densities because of the low eutectic temperature and the instability of M'-phase. Therefore, we may conclude that Dy_2O_3 is the most reliable sintering additive to use for α-sialon-based ceramics, to achieve an optimum combination of hardness, strength and toughness over extended periods of time at temperatures in excess of 1650 °C.

Acknowledgement

One of us (H.M.) acknowledges financial assistance from the Engineering and Physical Sciences Research Council (EPSRC) during the course of this work.

References

1. G. Z. CAO and R. METSELAAR, *Chem. Mater.* **3** (1991) 242.
2. T. EKSTRÖM, in "Proceedings of Austceram'92, Key Engineering Materials", Vols 53–55, edited by P. J. Darragh and R. J. Stead (Trans Tech, Switzerland, 1991) p. 586.
3. K. H. JACK, *J. Mater. Sci.* **11** (1976) 1135.
4. S. HAMPSHIRE, H. K. PARK, D. P. THOMPSON and K. H. JACK, *Nature* **274** (1978) 880.
5. T. EKSTRÖM and I. INGELSTRÖM in "Proceedings of the Non-oxide Technical and Engineering Ceramics", Limerick, 1985, edited by S. Hampshire (Elsevier Applied Science, London, 1986) p. 231.
6. M. H. LEWIS, in "Proceedings of the Silicon Nitride 93, Key Engineering Materials", Vols 89–91, edited by M. J. Hoffmann, P. F. Becher and G. Petzow (Trans Tech, Switzerland, 1993) p. 333.
7. H. MANDAL, PhD thesis, University of Newcastle upon Tyne, UK (1992).
8. Y.-B. CHENG and D. P. THOMPSON, *J. Am. Ceram. Soc.* **77** (1994) 143.
9. H. MANDAL, Y. -B. CHENG and D. P. THOMPSON, in "Proceedings of the 5th International Symposium on Ceramic

Materials and Components for Engines", Shanghai, May 1994, edited by D. S. Yan, X. R. Fu and S. X. Shi (World Scientific, Singapore, 1995) p. 202.
10. Y. -B. CHENG and D. P. THOMPSON, *J. Eur. Ceram. Soc.* **14** (1994) 13.
11. H. MANDAL, D. P. THOMPSON and T. EKSTRÖM, *ibid.* **12** (1993) 421.
12. K. LIDDELL, MSc thesis University of Newcastle upon Tyne, UK (1979).
13. A. G. EVANS and A. CHARLES *J. Am. Ceram. Soc.* **59** (1976) 371.
14. R. A. L. DREW, PhD thesis, University of Newcastle upon Tyne, UK (1980).
15. H. MANDAL, D. P. THOMPSON and T. EKSTRÖM, in "Proceedings of the Special Ceramics 9", London, December 1990 (The Institute of Ceramics, Stoke-on-Trent, UK, 1992) p. 97.
16. H. MANDAL and D. P. THOMPSON, in "Proceedings of the IV ECerS Conference", Italy, October 1995, to be published.
17. H. MANDAL, D. P. THOMPSON and T. EKSTRÖM, in "Proceedings of the 7th Irish Materials Forum Conference", IMF7, Limerick, September 1991, "Key Engineering Materials", Vols 92–94, edited by M. Buggy and S. Hampshire (Trans Tech, Switzerland, 1992) p. 187.
18. H. MANDAL and D. P. THOMPSON, in "Proceedings of IV ECerS Conference", Italy, October 1995, to be published.

Received 1 May
and accepted 7 June 1995